Collection SFN **13**, 03001 (2014)
DOI: 10.1051/sfn/20141303001

Local probes of magnetism, NMR and μSR: A short introduction

Fabrice Bert

Laboratoire de Physique des Solides, Université Paris Sud 11, UMR CNRS 8502, 91405 Orsay, France

Abstract. NMR and μsr are powerful local probes of magnetism which often complement neutron studies. This article consists of a brief introduction to those two techniques at a basic level for phD students and reseachers having some knowledge in magnetism but none in resonance techniques. The aim is to provide the basic knowledge of the outcomes and issues of these techniques in order to understand the related litterature.

1. INTRODUCTION

The first detection of nuclear magnetic resonance (NMR) in a liquid by F. Bloch and in a solid by E.M. Purcell traces back to the end of world war II. This is not a coincidence since NMR relates to the interaction of electromagnetic waves in the radiofrequency range and matter, a problem which is central to the radar technology. Since then the technique has considerably evolved but most remarkably its application field has grown impressively from analytical chemistry to medicine, magnetic resonance imaging being nowadays the most popular application.

In comparison, the μSR technique, which acronym stands as well for muon spin resonance, rotation or relaxation, is rather recent and confidential. It is restricted to a few beam lines scattered in four large scale facilities in the world. Its application field is nonetheless rather large, ranging from chemistry and semiconductor physics to hydrogen storage and muon catalysed nuclear fusion. The main research field remains however magnetism and superconductivity which fully take advantage of the exquisite sensitivity of the muon to detect small magnetic fields.

Both NMR and μSR are local probe techniques which means that the nuclei or muon spins are probing the local fields in their close vicinity, typically at the atomic scale. Another specificity of these techniques is that they are sensitive to very low energy excitations, typically in the μeV range. These make them very complementary tools to bulk thermodynamic measurements like SQUID magnetometry or neutron and x-ray diffraction techniques.

The present article aims at giving a short introduction to these techniques focusing only on the magnetic properties of solids. To cite just a few reference books, the reader interested by applications in condensed matter may refer for NMR to the comprehensive textbook by C.P. Slichter [1] or the more practical presentation by E. Fukushima and B.W. Roeder [2] and for μSR to the concise review by S.J. Blundell [3] and the detailed textbook by A. Yaouanc and P. Dalmas de Réotier [4].

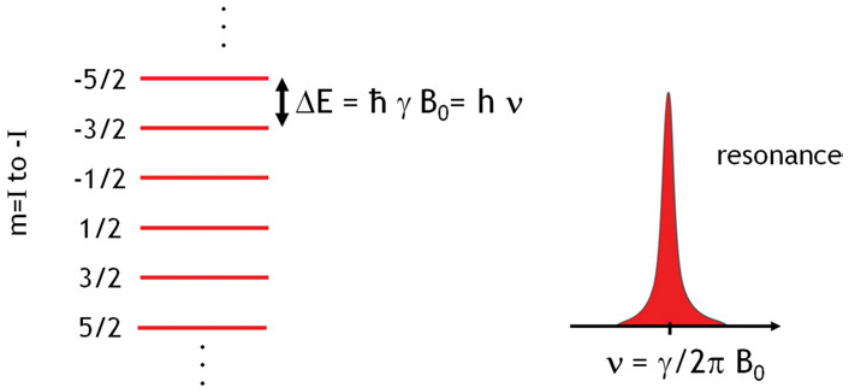

Figure 1. Scheme of the Zeeman splitting of the nuclear spin energy levels by a static magnetic field B_0 and the single resonance line corresponding to the inter-level ($I - 1 \longleftrightarrow I$) transitions.

NMR and μSR techniques are introduced successively in chapter 2, 3 and 4, 5. This separation may hide the similarity of the two techniques which appears more clearly in chapter 6 dedicated to measurements of spin dynamics where the same formalism applies for both NMR and μSR.

2. NMR PRINCIPLES

2.1 Zeeman effect

Nuclear magnetic resonance is fundamentally a very accurate measurement of the Zeeman splitting of the energy levels of the nuclear spin in a static magnetic field. Consider a nucleus with a spin I. Its magnetic moment is $g_n \mu_n I$ where μ_n is the nuclear magneton or alternatively $\hbar\gamma I$ where γ is the gyromagnetic ratio of the nucleus. In an applied field B_0, the $2I + 1$ levels are equally split by the amount $\Delta E = \hbar\gamma B_0$. An NMR experiment consists in inducing transitions between the Zeeman split levels with an electromagnetic wave. This happens at "resonance", *i.e.* when the frequency of the wave matches the energy difference between two consecutive levels

$$\nu = \frac{\gamma}{2\pi} B_0. \tag{2.1}$$

For the nuclei which possess a spin, the gyromagnetic ratio $\gamma/2\pi$ is in the range 0.729 MHz/T (for ^{197}Au) to 42.57 MHz/T (for the proton ^{1}H), so that for standard laboratory magnetic fields of the order of 10 T, the resonance falls in the radiofrequency range.

The outcome of the measurement is an histogram – the NMR spectrum – which displays the number of nuclei resonating at ν as function of ν. It can be also viewed from Eq. (2.1) as the plot of the distribution of the magnetic fields existing in the sample. Thus, in a non magnetic material, the spectrum reveals the external field profile in the sample and indeed high resolution teslameters are actually based on NMR. More interesting to us is the case of magnetic materials which possess either static moments or some finite polarization induced by the external field. Then the nuclei probes not only the applied field B_0 but also internal fields so that the resonance frequency is shifted with respect to the reference value corresponding to $\gamma B_0/2\pi$. We will describe later how the nuclear spin is coupled to the surrounding electronic spins, but it is worth noting already that the NMR line shift and the NMR line shape reveal the internal field distribution and therefore the static magnetic properties of the sample. It is also worth noting that two nuclei experiencing different field give separate resonance lines in the NMR spectrum, whatever the distance in real space between them. Thus, although there is no direct spatial information

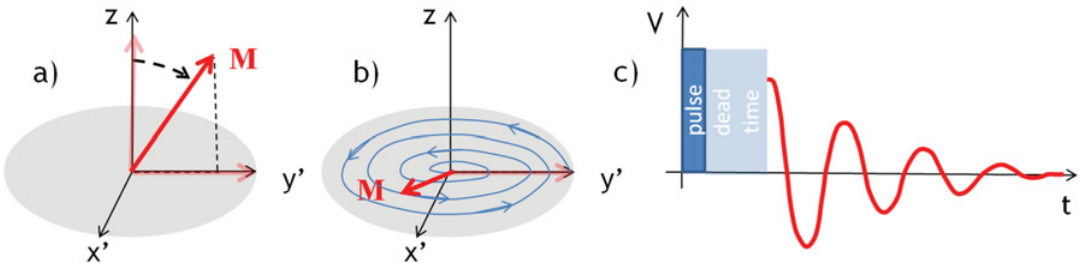

Figure 2. The nuclear magnetization **M** is initially along the applied static field $\mathbf{B}_0$ (z direction). After a $\pi/2$ pulse (a), it lies in the plane perpendicular to $\mathbf{B}_0$ and precesses at the Larmor frequency (b). Meanwhile the magnetization decreases because of T_2 relaxation effects. (c) Voltage detected at the ends of the small detection coil, the same one which was used to produce the excitation pulse.

in the NMR spectrum, the spatial resolution of the measurement is the atomic scale and therefore one speaks of local probe technique.

2.2 Pulsed NMR

Nowadays an NMR experiment really means a *pulsed* NMR experiment, *i.e.* the resonance line is measured by sending one or several pulses of radiofrequency wave rather than recording the absorption of a continuous wave. As we shall see in the following, the advantage is twofold; first, by using pulses one can manipulate at will the nuclear magnetization to measure not only the NMR spectrum but also independently the dynamics and second it allows to irradiate the sample at the same time with a whole range of frequencies rather than just one and therefore to use Fourier transform analysis.

The evolution of a nuclear magnetic moment $\boldsymbol{\mu}$ in a magnetic field **B** is given by the equation of motion[1]

$$\frac{d\boldsymbol{\mu}}{dt} = \gamma \boldsymbol{\mu} \wedge \mathbf{B} \tag{2.2}$$

which simply describes the precession of the moment at its natural frequency $\frac{\gamma}{2\pi}B$, called the Larmor frequency, around **B** when the magnetic field is static. In a pulse NMR experiment, in addition to the $\sim$10 T static field $\mathbf{B}_0$, a much smaller $\sim$0.01 T oscillatory magnetic field $\mathbf{B}_1$ is applied during a short duration $t \sim 1\,\mu$s, perpendicularly to $\mathbf{B}_0$. This additional field is produced by a small resistive coil surrounding the sample. At resonance, and *only* at resonance, when the frequency of $\mathbf{B}_1$ matches the Larmor frequency, it is easy to see that, in the frame rotating at the speed γB_0, the effect of $\mathbf{B}_1$ is to rotate the nuclear moment by an angle $\gamma B_1 t$ with respect to $\mathbf{B}_0$ (see Fig. 2). Thus from an initial configuration where the moment is along $\mathbf{B}_0$, by playing on the duration of the radiofrequency pulse, the moment can be made to lie in the plane perpendicular to $\mathbf{B}_0$ ("$\pi/2$ pulse") or even to become antiparallel to $\mathbf{B}_0$ ("π pulse"). The corresponding pulse duration is of the order of 1 μs.

After a $\pi/2$ pulse, the moment precesses freely around $\mathbf{B}_0$. It induces an oscillatory flux in the same small coil that has been used to produce the pulse. In an experiment one is dealing with an assembly of many such magnetic moments which sum up to build the nuclear magnetization **M**. Although the latter magnetization is very small compared for instance to the electronic magnetization (typically 10^6 smaller), the resulting total flux can still be large enough to become detectable. The NMR signal is the voltage at the small reception coil, *i.e.* it is proportional to the time derivative of the nuclear

[1] We use here for simplicity a classical treatment. Similar expressions are found in the quantum case by replacing the classical moment by the expectation value of the moment operator.

magnetization. At working temperatures, the interaction between nuclear spins is certainly negligeable and their magnetization is simply given by the Curie-Law, thus proportional to $\gamma^2 B_0/T$. Time-derivative yields an additional γB_0, so that eventually the NMR signal is proportional to $\gamma^3 B_0^2/T$. It follows that strong external fields are highly recommended, at least in situations where there are no field induced effects, and so is low temperature. It also explains the huge difference of NMR sensitivity depending on the probed nuclei through its γ. The signal to noise ratio in an NMR experiment remains intrinsically poor but this is merely a technical problem. The measurement is eventually possible because the nuclear response is not hindered by the electronic one as in standard magnetometry, it is measured in isolation thanks to the selectivity of the resonance method. More challenging is the use of the same coil for excitation and reception. It demands a very good isolation of both circuits given that the excitations pulses, in the 100 V range, are $\sim 10^8$ larger that the voltage associated to the flux variation produced by the nuclei. The reception is nonetheless blinded during a short time after the pulse, called the "dead time". The dead time cannot be reduced much below a few μs.

After the $\pi/2$ pulse, precession does not carry on for ever. Because the nuclear moments are not isolated but interact with their environment which includes other nuclear spins, and electrons, the nuclear magnetization eventually relaxes to its equilibrium position, along $\mathbf{B}_0$. In addition to Eq. (2.2), one needs to introduce relaxation processes to fully describe the evolution of the magnetization. This is concisely summarized in the so-called Bloch equations

$$\frac{\partial M_x}{\partial t} = \gamma M_y B_0 - \frac{M_x}{T_2} \tag{2.3}$$

$$\frac{\partial M_y}{\partial t} = -\gamma M_x B_0 - \frac{M_y}{T_2} \tag{2.4}$$

$$\frac{\partial M_z}{\partial t} = \frac{M_0 - M_z}{T_1} \tag{2.5}$$

where M_0 is the equilibrium magnetization and two different relaxation times are introduced. T_2 is the shortest one and characterizes the relaxation of the transverse magnetization. It arises first because all nuclear spins do not experience exactly the same static field. They do not precess exactly at the same speed and therefore the total transverse magnetization decreases with time. In addition the interactions between nuclear spins provide incoherent relaxation processes which do not change the energy of the nuclear spins system but lead to a decrease of the transverse magnetization. On the contrary, all processes which allow an energy exchange between the nuclear spins and the environment contribute to T_1, the so called "spin-lattice" relaxation. We will come back to this latter relaxation time which directly probes the excitation spectrum in a magnetic material. This relaxation time sets the NMR experiment time scale since one has to wait that the relaxation is back to its equilibrium position before sending another excitation pulse. Relaxation times can be as large as hours in non magnetic insulators or shorter than the dead time in case of a strong weight of low energy excitations, for instance in the critical slowing down regime close to a magnetic transition. In the latter case, the experiment is simply not possible. Somehow counterintuitively, the advantage of NMR over other local probes like ESR is that the nucleus is poorly coupled to the environment so that relaxation times do not often get too short. In magnetic materials, to further reduce this coupling it is often useful to perform NMR on a nucleus which does not belong to the magnetically active ion.

As already mentioned, a second advantage of pulsed NMR is the possibility to use the power of Fourier transform analysis. Indeed the Fourier transform of a square pulse of length τ of a pure $\sin(2\pi\nu_0 t)$ signal is a cardinal sine of typical width $1/2\tau$ (this width is defined so that the Fourier components vary by less than 10% with respect to the maximum one at ν_0). Therefore the detected NMR signal contains the system response to this whole range of excitation frequencies around ν_0. The signal can then be

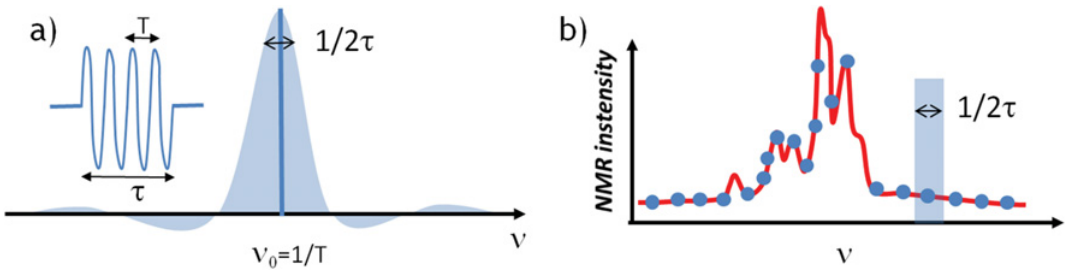

Figure 3. a) Fourier spectrum of the excitation radiofrequency pulse depicted in the inset. b) Complex NMR spectrum (solid line) reconstructed from the combination of a few individual Fourier spectra measured at various discrete frequencies shown by circles. The shaded area represents the frequency window which is irradiated efficiently in one single experiment at a given frequency.

analyzed by Fourier transform. If the NMR spectrum width is smaller than $1/2\tau$, it can thus be measured in one single experiment. Otherwise one has to perform several measurements with a frequency step $\sim 1/2\tau$ and then combine several Fourier transforms (see Fig. 3). This technique is especially useful when the spectrum consists of multiple narrow lines.

3. NMR SHIFT AND LOCAL SUSCEPTIBILITY

In this section, we introduce the hyperfine coupling between nuclei and electrons. It results in a shift of the NMR line which is related to the electron susceptibility. Examples are given to illustrate the local character of the susceptibility measured in an NMR experiment, in contrast to the macroscopic susceptibility measured with standard magnetometers.

3.1 Hyperfine coupling

The interaction between a nuclear spin $\mathbf{I}$ and the spin $\mathbf{S}$ of a surrounding electron is called the hyperfine coupling and is expressed by the Hamiltonian

$$\mathcal{H} = \mathbf{I}.\overline{A}.\mathbf{S} \tag{3.1}$$

where $\overline{A}$ is the hyperfine tensor. This concise expression hides a variety of different microscopic mechanisms which may occur simultaneously. Depending on the filling of the electronic shell, the nature of the electron orbital, whether the unpaired electrons belongs or not to the same atom as the nucleus, etc. the coupling can be strong or weak, isotropic or anisotropic. In case of an s electron, the hyperfine interaction is isotropic (scalar) and usually very strong. The s shell needs not to be half filled to contribute. Even when full, it can be slightly polarized by unpaired electrons belonging to other orbitals, a mechanism which is termed "core polarization". For electrons belonging to other shells (p,d,f..), the interaction is dipolar and $\overline{A}$ is anisotropic.

The Hamiltonian 3.1 can be conveniently rewritten

$$\mathcal{H} = -\hbar\gamma_I \mathbf{I}.\left[\frac{\overline{A}}{\hbar^2\gamma_I\gamma_e}.(-\hbar\gamma_e\mathbf{S})\right] = -\boldsymbol{\mu}_I.\mathbf{B}_{loc} \tag{3.2}$$

so that it appears as the interaction between the nuclear moment $\boldsymbol{\mu}_I = \hbar\gamma_I\mathbf{I}$ and an effective hyperfine field $\mathbf{B}_{loc}$ which depends on the electronic moment $-\hbar\gamma_e\mathbf{S}$, γ_e being the electron gyromagnetic ratio. The subscript of $\mathbf{B}_{loc}$ reminds us that only local electrons, in the direct vicinity of the nucleus contribute. On the time scale of the NMR experiment, the electronic spin fluctuations cancel out and only the average

value $\langle \mathbf{B}_{loc} \rangle$ is detected. This local static field adds to the external field so that the nuclear resonance will be *shifted* from the reference $\gamma_I B_0/2\pi$ by the amount

$$\nu = \gamma_I(B_0 + B_{loc}) = \nu_0(1 + K_s) \tag{3.3}$$

where

$$K_s = \frac{\nu - \nu_0}{\nu_0} = \frac{B_{loc}}{B_0} \tag{3.4}$$

which is termed the hyperfine shift.

In a magnetically frozen phase, the shift relates to the static electronic moments and therefore tracks the order parameter. In a paramagnetic phase, B_{loc} relates to the uniform ($\mathbf{q} = 0$) local susceptibility χ_{loc} of the electrons in the close vicinity to the probed nucleus, *i.e.* those that are coupled through $\overline{A}$. From Eq. (3.2) and introducing the density of unpaired electrons n, we get[2]

$$B_{loc} = \frac{\mu_0 A}{\hbar^2 \gamma_I \gamma_e n} \chi_{loc} B_0 \tag{3.5}$$

which shows that the shift is then proportional to the local susceptibility

$$K_s = A_{hf} \chi_{loc}, \quad \text{with} \quad A_{hf} = \frac{\mu_0 A}{\hbar^2 \gamma_I \gamma_e n} \cdot \tag{3.6}$$

In the litterature, the hyperfine coupling is either given in energy unit according to the definition 3.1 or, quite often, in Oersted, then referring to the definition $K = A'\chi/\mu_B$ where χ and μ_B should be expressed in cgs units. In addition to the electron spin contribution (Eq. (3.1)) which is of major interest to the study of magnetic materials, the electronic orbital also contributes to the nuclear spin energy and therefore to the lineshift. This latter contribution K_{orb} is weak, temperature independent but depends on the orbital type. It is thus at the heart of the use of NMR for chemical analysis. In the end, the total lineshift is

$$\nu = \nu_0(1 + K_s + K_{orb}). \tag{3.7}$$

One other important interaction which we will not describe here is the one with the electric field gradient which provides (local) structural informations. The interested reader can refer to the comprehensive treatment by M.H. Cohen and F. Reif [5].

3.2 Local susceptibility: Defect induced staggered magnetization

A striking demonstration of the local nature of the NMR technique is the measure of the local response of a magnetic system to a defect. In most correlated system, this response takes the form of a staggered magnetization which extension and magnitude depend on (and reveal) the correlations of the unperturbed system. Such a response has been observed by NMR in many systems including spin chains, ladders, superconducting cuprates, spin glass diluted alloys. The interested reader may refer to the review by H. Alloul *et al.* [6].

As an example of such measurements, Figure 4 shows ^{89}Y NMR in the Y_2BaNiO_5 compound. In this insulator, only the Ni^{2+} ions (S = 1) bear a magnetic moment. It is considered as a prototype Haldane spin chain material, namely a (quasi) one-dimensional S=1 Heisenberg antiferromagnet. Interestingly, Y_2BaNiO_5 can be prepared in a rather pure form and then doped in a controled manner on the Ni site, either by non-magnetic (Mg^{2+}, Zn^{2+}) or magnetic (Cu^{2+}, $S = 1/2$) ions [7, 8]. Strikingly, in the NMR spectrum of the doped compound, additional weight appears on the wings of the NMR spectrum. The so-called "satellite" additional lines are strongly shifted with respect to the main line which evidences

[2] For simplicity we use from now on a scalar hyperfine coupling and a scalar susceptibility. In reality both quantities may be tensorial.

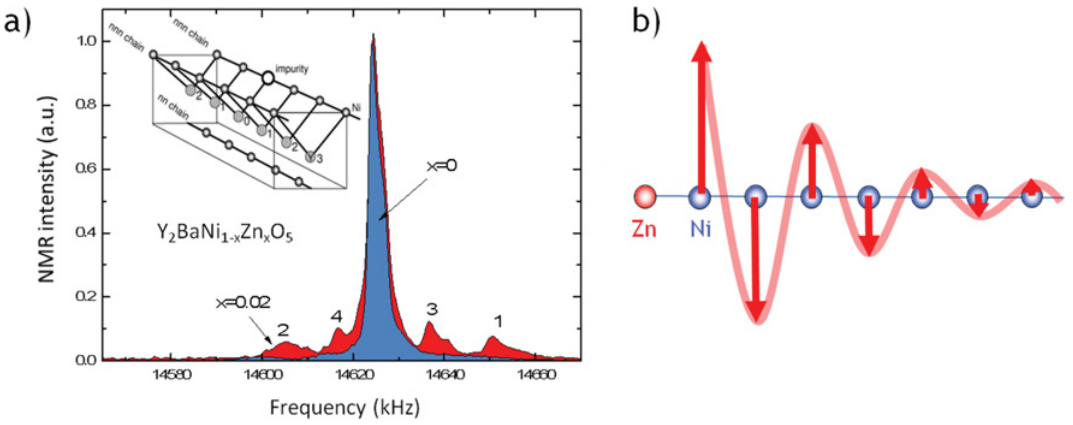

Figure 4. a) Comparison of the ^{89}Y NMR spectra of the spin 1 chain Y_2BaNiO_5 compound with and without 2% non-magnetic zinc doping. The inset shows the location of the ^{89}Y nuclei with respect to the Ni magnetic chains. Each ^{89}Y is mainly hyperfine coupled to two next nearest neighbor chains (*nnn*) and not to the nearest one (*nn*). The Y ions are labeled as a function of their distance to one spin vacancy impurity on one *nnn* chain. Each type of Y corresponds to a given satellite line in the NMR spectrum. b) Scheme of the local staggered magnetization induced in the vicinity of a non-magnetic Zn dopant.(Adapted from [7]).

that some of the ^{89}Y nuclei experience a much stronger local field than the majority ones. Moreover, these satellite lines appear on both sides of spectrum. Thus, for some of the nuclei the additional strong local field is along the direction of the applied magnetic field while for some of them it has to be in the opposite direction. This clearly evidence the existence of a staggered magnetization induced by the spin vacancy.

In such a clean case, one can readily assign the satellite lines to the Y ion location with respect to the defect. Namely, the further the satellite is from the main central line, the closer the Y ion is to the non magnetic impurity. On the other hand the main line tracks the unperturbed behavior, far from the dopant. Provided that the hyperfine couplings are well known, such an experiment provides a set of local susceptibilities as a function of the distance to the impurity which can each be measured versus temperature. These results can then be quantitatively compared to theoretical models and give precious information on the correlation at play in the material. In the most common less clean cases, for higher doping rate or in case of a broader central line in the pure compound, the satellites are not resolved. Only an additional broadening of the NMR line is detected. In this case the NMR lineshape reflects the distribution of local susceptibilities.

4. μSR PRINCIPLES

Muons are light elementary particles, about 9 times lighter than a proton, with a finite lifetime of 2.2 μs. They can be either positively or negatively charged, but in most condensed matter experiments, only positively charged μ^+ are used. Indeed μ^- bind too tightly to the nuclei in matter to be good probe of the electronic properties. Muons also possess a S=1/2 spin and most interestingly for the study of magnetic properties, they bear a large magnetic moment about 3 times the proton one ($\gamma_\mu/2\pi = 135.5\,\mathrm{MHz/T}$), hence their strong sensitivity to magnetic fields. They exist naturally in cosmic rays but condensed matter experiments yield stronger fluxes available only in large scale facilities. There are currently four such muon sources at the Paul Scherrer Institut (PSI, Switzerland), the Tri-University Meson Facility (TRIUMF, Canada), the High Energy Accelerator Research Organization (KEK, Japan) and the Rutherford Appleton Laboratory (ISIS, UK). Muons are produced during the two body decay of

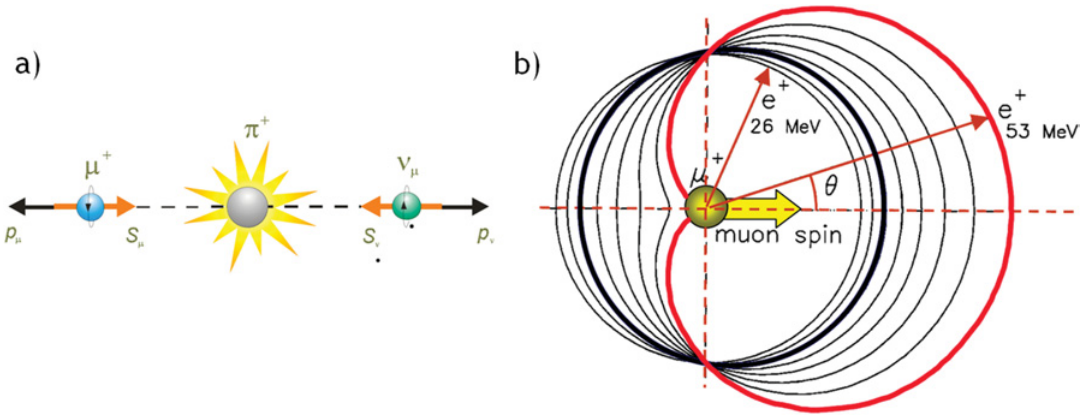

Figure 5. a) Schematic of the pion decay into a muon and a neutrino. In the case where the pion was initially at rest, because of the momentum conservation law, both particles are emitted with their spin aligned antiparallel to their momentum. b) Angular dependence of the probability of emission of a positron during the muon decay. The higher the energy of the emitted positron, the more asymmetric the positron emission.

pions (see Fig. 5a) which are themselves produced from the impact of a proton beam onto a graphite target. Given that pions bear no spin and that neutrinos always have their spin antiparallel to their momentum, by selecting only those pions which are at rest in the target before decaying, a 100% polarized muon beam is produced. This is a main difference and an interesting advantage over NMR, since here no external field is required and the magnetic properties can be investigated in zero field. A second consequence is that, contrary to NMR, the sensitivity of a μSR experiment does not depend either on temperature.

The produced muon beam is directed to the sample where muons stop. The stopping process is fast, on the nanosecond time scale, and importantly involves only electrostatic interactions which preserves the initial polarisation of the muons. Depending on the number of cryostat windows the muons have to cross before reaching the sample, about 100 to 200 mg/cm^2 of matter is needed to stop the muon. Thus, for usual material, muons stop at a few 10 μm from the surface, so that μSR is indeed a *bulk* technique. Note that contrary to x-rays or neutrons, muons are not reflected nor diffracted, they merely stop into the sample and stay there, at rest[3]. Being positively charged, μ^+ stop in an electrostatically favorable site in the unit cell. For instance in $YBa_2Cu_3O_7$ cuprate, J.H. Brewer *et al.* have carefully determined that μ^+ sit at about 1 Å away from one of the oxygen ions [9]. In most cases, the muon location is however not known accurately which constitutes a major limitation of the technique.

During their lifetime in the sample, the muon spins may loose their initial polarization because of the presence of static or dynamical internal fields. In a μSR experiment, this is this relaxation of the initial polarization versus the time spent by the muon in the sample that one wants to measure. The muon decay gives rise to one positron and two neutrinos. As shown in Figure 5b, μSR relies on the asymmetry of the positron emission, the latter being emitted preferentially in the direction of the muon spin just before its decay. The muon decay being a three body process, the positron energy may vary between 0 and the mass energy of the muon, 53 MeV. Most positrons have enough kinetic energy to leave the sample and reach photomultiplier detectors located outside the sample environment (cryostat, pressure cell...).

A clock is started when the muons get to the sample, defining the time $t = 0$ of the experiment. One event consists of the detection of one positron in a detector at the time t of the muon decay. The data

[3] In some cases, muon may diffuse in the sample, usually at high temperature through activated hopping processes, but also through quantum tunneling at low temperature, for instance in simple metals.

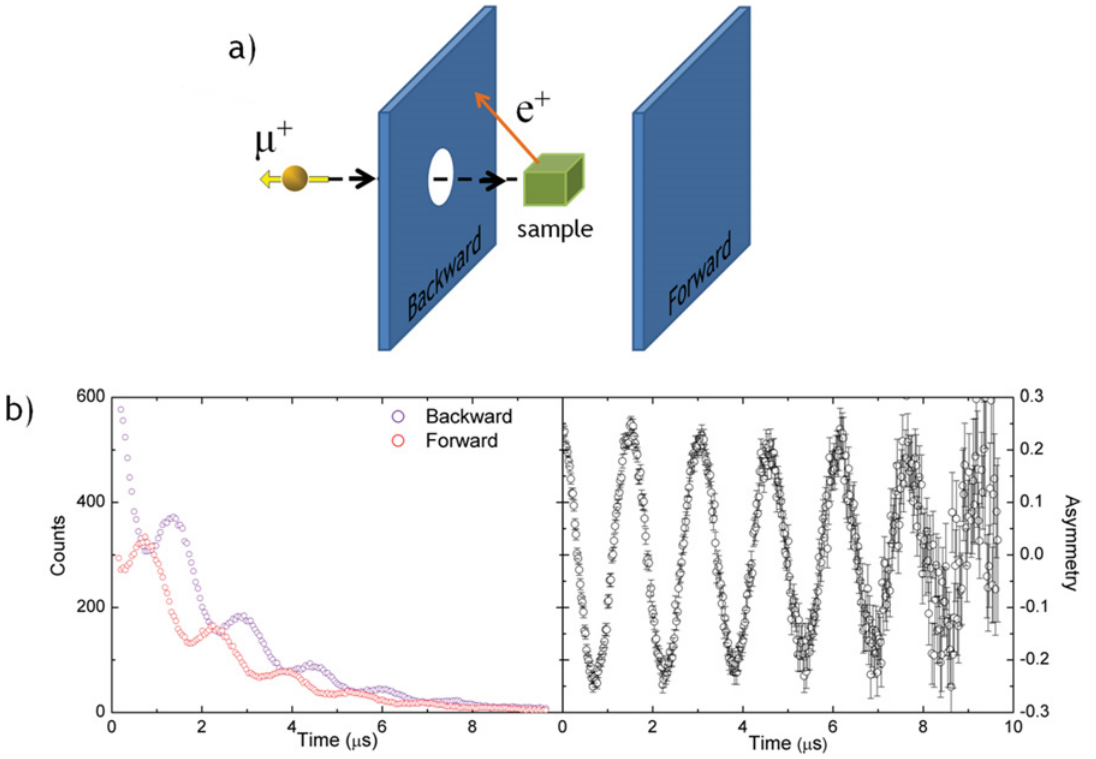

Figure 6. a) Schematic of a μSR longitudinal experimental setup. b) (Left) number of positrons collected in backward and forward detectors as a function of the time elapsed since the muon implantation. In this experiment an external field of 0.005 T was applied in a direction perpendicular to the initial muon spin polarization giving rise to a well defined precession signal. (Right) asymmetry of the muon decay computed from the individual counter data.

set, as shown in Figure 6b, is the histogram of all such events. The exponential decrease of the number of events with time reflects the finite 2.2 μs lifetime of the muon. Thus the statistics becomes very poor at long times and the typical musr time window does not exceed 10–20 μs. In order to get rid of the exponential decay law and emphasize the variation of the muon polarization in isolation, one usually computes the asymmetry of the muon decay

$$a(t) = \frac{N_B(t) - \alpha N_F(t)}{N_B(t) + \alpha N_F(t)} \tag{4.1}$$

where $\alpha \sim 1$ accounts for the dissymmetry of the detectors, located on both sides of the sample – the so-called Forward and Backward detectors in the longitudinal setup[4] sketched in Figure 6a. A more fundamental quantity which is also often used in litterature, but which necessitates some further manipulation, is the muon polarization

$$P(t) = \frac{a(t) - B}{a(0) - B}, \tag{4.2}$$

[4] When large transverse fields are applied, a better suited configuration consists in having the detectors parallel to the beam. This so-called transverse configuration is used for instance for muon shift experiments or penetration depths measurements in supraconductors. We will not describe this kind of experiments here.

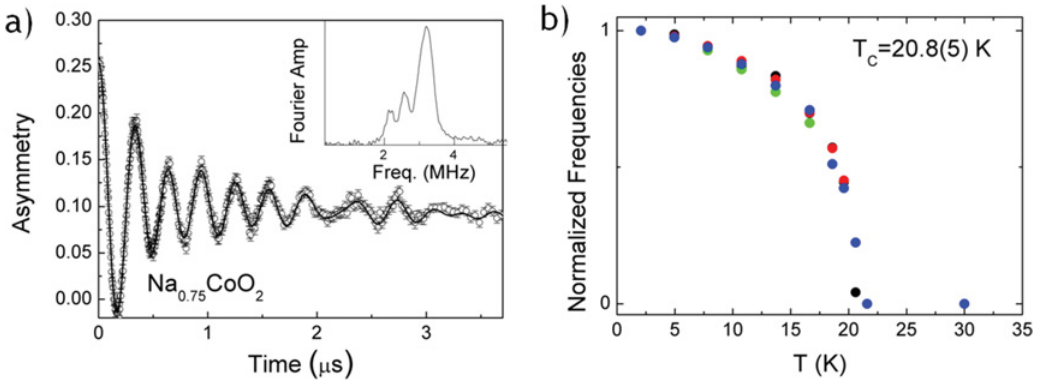

Figure 7. a) Zero-field muon decay asymmetry measured in the magnetically ordered phase of the $Na_{0.75}CoO_2$ cobaltate. The spontaneous oscillation evidences the presence of well defined internal fields. Note the constant asymmetry at long time, ca. one third of the initial asymmetry, which is a strong signature of fully static magnetism. The solid line is a fit to Eq. (5.3) with 4 frequencies $\gamma_\mu B^i_{loc}$ hence 4 muon sites. The inset shows the Fourier transform of the asymmetry. The three well-defined peaks correspond to the four different muon stopping sites, two of them with slightly different frequencies which are not resolved in the high frequency Fourier peak. b) Evolution of the frequencies of the spontaneous oscillations of the asymmetry with temperature, rescaled to their base temperature value. All frequencies fall on top of each other showing that all muon probe the same magnetism whatever their stopping site (Adapted from [10]).

where B stands for the constant background contribution of those muons stopping outside the sample of interest, for instance in the sample holder.

5. DETECTION OF STATIC MAGNETISM WITH ZERO-FIELD μSR

At variance with NMR, muons are only sensitive to magnetism, there are no quadrupolar effects. The main coupling of the muon spin to the neighboring unpaired electrons is usually dipolar. In this respect μSR is a less local technique than NMR. Thanks to the large gyromagnetic ratio γ_μ of muons and the full polarization of the muon beam, μSR is particularly well suited to track static internal fields as low as a fraction of one Gauss. Such small internal fields typically correspond through the dipolar coupling to frozen electronic moments lower than $0.01\mu_B$.

In a magnetically frozen material, the implanted muon experiences a static internal field $\mathbf{B}_{loc}$ around which its moment precesses at the speed $\gamma_\mu B_{loc}$. If $\mathbf{B}_{loc}$ makes an angle θ with respect to muon beam direction, then the muon polarization evolves according to

$$P(t) = \cos^2\,\theta + \sin^2\,\theta \cos(\gamma_\mu B_{loc} t). \tag{5.1}$$

In case of long range magnetic order, and only in this case, all muons stopping at the same crystallographic site experience the same local field. Thus they all have their polarization evolving according to Eq. (5.1) and so does the measured macroscopic polarization. The observation of a spontaneous oscillation of the polarization with time in zero external field is an unequivocal signature of long range order. The frequency of this oscillation is a direct measurement of the internal field, *i.e.* of the order parameter.

An illustration of such a case in provided in Figure 7. As in many other families of compounds, μSR has proven to be a very fast and efficient technique to unravel the complicate magnetic phase diagram of sodium cobaltates Na_xCo0_2 as a function of the Na content and temperature. In this simple example, antiferromagnetism sets in at 20.8(5) K in the $Na_0.75CoO_2$ compound [10] and the order parameter merely increases upon cooling down without subsequent transitions. The investigated sample being

polycrystalline, one has to calculate the resulting powder averaged polarisation. This is readily done by integrating Eq. (5.1) over the isotropic distribution $p(\theta) = \frac{1}{2}\sin\theta$ of $\mathbf{B}_{loc}$ with respect to the muon beam direction, which leads to

$$P(t) = \frac{1}{3} + \frac{2}{3}\cos\left(\gamma_\mu B_{loc} t\right). \tag{5.2}$$

The measured asymmetry shown in fig. 7.a consists of several oscillatory signals of the form 5.1, which evidences the existence of several muon stopping sites, hence of various distinct local fields. Eventually the asymmetry can be fit to

$$a(t) = (a(0) - B)P(t) + B = (a(0) - B)\left(\frac{1}{3} + \frac{2}{3}\sum_i f_i \cos\left(\gamma_\mu B^i_{loc} t\right)\exp(-t/2\sigma_i)\right) + B \tag{5.3}$$

where the initial asymmetry is $a(0) \sim 0.26$ and the constant asymmetry of muons falling in a silver sample holder is $B \sim 0.02$. The sum runs over the different muon stopping sites, f_i is the fraction of the muons stopping at site i where the magnitude of the dipolar field arising form the cobalt ions is B^i_{loc}. The gaussian damping accounts for a small distribution of the local fields.

In the other limit of random static fields, each muon experiences a different local field. The full polarization is obtained by integrating Eq. (5.1) over both θ and the amplitude of the local field. The well known Kubo-Toyabe formula

$$P(t) = \frac{1}{3} + \frac{2}{3}(1 - \gamma_\mu^2\Delta^2 t^2)\exp(-\gamma_\mu^2\Delta^2 t^2/2) \tag{5.4}$$

corresponds to a gaussian field distribution of width Δ centered around 0. Such a distribution arises in the case of a dense set of random magnetic moments, a good realization of which is nuclear magnetism. Indeed the dipolar interaction between nuclear moments is very small so that they fluctuate very slowly and can be considered static on the muon lifetime time-scale. The nuclear fields when they exist are usually in the Gauss range, well detectable in the μSR time window. The nuclear contribution of the form 5.4 often dominates the relaxation of the muon decay asymmetry in the high temperature limit, when electronic moments usually fluctuate fast. That is the reason why silver, which bears tiny nuclear moments, is a first choice sample holder material in μSR experiments.

Another case of randomness is provided by spin glasses. However in most textbook cases of diluted magnetic alloys, the field distribution is rather lorentzian. At variance with formula 5.4, the corresponding lorentzian Kubo-Toyabe formula is not gaussian-like at early times and the dip at $t \sim 1/\gamma_\mu\Delta$ is less pronounced. In any case, static random magnetism is characterized by one strongly damped oscillation followed by a constant $1/3^{rd}$ polarization at long times, the so-called *$1/3^{rd}$ tail*. Eventually, for powder samples, the presence of a $1/3^{rd}$ tail is a strong evidence for static magnetism, whatever random or long range order.

6. SPIN DYNAMICS

So far we have been considering only the time-averaged values of the local fields probed either by the muon or nucleus spin. These average values reflect the static magnetic properties of the studied material. As already mentioned at the end of Section 1.2 when introducing Bloch equations to describe the evolution of the nuclear magnetization, the fluctuations of the local fields contribute to dynamical relaxation processes which relate to electronic spin dynamics and which can also be probed with both techniques.

In the simplest cases of a nuclear spin $I = 1/2$, the relaxation is exponential $M_z(t) = M_0 e^{-t/T_1}$ with one single parameter, the spin-lattice relaxation time T_1, containing all the information about the relaxation processes. For higher nuclear spin values $M_z(t)$ is combination of exponential terms but

still with one single parameter T_1. Similarly for a homogeneous fully dynamical system, the muon polarization relaxes exponentially $P(t) = e^{-\lambda t}$ where the relaxation rate $\lambda \equiv 1/T_1$ is introduced as usually done in litterature.

By using the Fermi-Golden rule to calculate the transition rate between nuclear or muon spin levels induced by the time-dependant local fields, *i.e* with the Hamitonian (3.2)[5], one gets

$$\frac{1}{T_1} = \frac{\gamma^2}{2} \int_{-\infty}^{+\infty} \langle \mathbf{B}_{\text{loc}}^{+}(t) \mathbf{B}_{\text{loc}}^{-}(0) \rangle e^{-i\omega_L t} \mathrm{d}t \tag{6.1}$$

where the brackets stand for statistical averaging, γ is the gyromagnetic ratio, either of muon or of the probed nucleus and $\omega_L = \gamma B_0$ the Larmor frequency in the applied longitudinal field. This expression makes clear that only the fluctuations of the transverse components of the local fields $\mathbf{B}_{\text{loc}}^{\pm}$ contribute to the relaxation process.

Expressing the local field as a function of the neighboring spins to which nuclei or muons are coupled,

$$\mathbf{B}_{\text{loc}} = \sum_i \frac{1}{\hbar\gamma} \overline{A}(\mathbf{r_i}).\mathbf{S}(\mathbf{r_i}, t) \tag{6.2}$$

and using the fluctuation dissipation theorem, one gets another useful expression of T_1[6]

$$\frac{1}{T_1} = \frac{k_B T}{\hbar^2} \sum_{\mathbf{q}} |A(\mathbf{q})|^2 \frac{\chi_{\perp}''(\mathbf{q}, \omega_L)}{\omega_L} \tag{6.3}$$

which makes a direct connection with the imaginary part $\chi''(\mathbf{q}, \omega)$ of the susceptibility that is measured in an inelastic neutron scattering experiment. However, note that here, as a consequence of the local nature of the techniques, $1/T_1$ is not $\mathbf{q}$ selective; all the wave vectors contribute. Also, one should remember that $\hbar\omega_L$ is extremely low, of the order of μeV so these relaxation measurements probe only the low energy excitations, in an energy range unavailable to neutron experiments.

A simple and enlightening case is that of an exponentially decaying local field correlation function

$$\langle \mathbf{B}_{\text{loc}}^{+}(t) \mathbf{B}_{\text{loc}}^{-}(0) \rangle = \Delta^2 e^{-\nu t}, \tag{6.4}$$

where all the dynamics is characterized by one single frequency ν and Δ is the second moment of the distribution of the transverse local fields. Using the expression (6.1), one computes

$$\frac{1}{T_1^{\mu}} = \frac{\gamma^2 \Delta^2 \nu}{\nu^2 + \gamma^2 B_0^2} \tag{6.5}$$

which is known as the Redfield theory (see for instance [1]) or the BPP formula from its discoverers M. Bloembergen *et al.* [11]. In the fast fluctuation limit, when $\nu \gg \gamma B_0$, one simply gets $T_1 \propto \nu$. Thus a slowing down of the spin dynamics while cooling down, for instance in the vicinity of a magnetic transition, translates into an increase of the relaxation rate $\lambda \equiv 1/T_1$. Given that deep inside the magnetic phase $1/T_1$ gets very small due to vanishing magnetic excitations, one expects and indeed observes a peak of $1/T_1$ at the transition temperature.

---

[5] The Hamiltonian has been introduced for nuclear spins in section 3.1 but the same formalism applies to the muon spin interaction with neighboring electronic spins. In this latter case, $\overline{A}$ often reduces to a dipolar tensor only.

[6] Here we restrict to scalar interactions and susceptibility.

7. CONCLUSION

μSR and NMR are thus two complementary techniques to investigate magnetic properties. The great advantage of muons is that they can be implanted in any materials and that the sensitivity of the measurement does not depend neither on the material nor external conditions such as temperature or applied magnetic field. The related drawback is that the technique relies on the implantation of a charge defect, the muon, in the material at some location not known with great accuracy. How far the muon modifies its local environment is a question that one has always to bear in mind, especially when dealing with subtle magnetic ground states. μSR is particularly well-suited to track very low frozen moments, for instance in matter with strong quantum fluctuations. It is a very efficient technique to draw the contour of magnetic phase diagrams. The detailed nature of the phases is less easy to investigate, both because of the local nature of the technique and because of the inaccuracy on the muon location. Regarding dynamics, in μSR, due to the short time window – a few nanoseconds to 10–20 μs – and the relatively small dipolar coupling, ca. $0.1\,\mathrm{T}/\mu_B$, slow electronic spin fluctuations down to the MHz range can be measured. In NMR the sensitivity and even the possibility of doing an experiment strongly depends on the available nuclei and/or the possibility of isotopic enrichment. For magnetic materials, one drawback is in most cases the need to apply an external field which can play a role in the physics of the investigated sample, especially at low temperature. Quite generally the time scale to perform an NMR experiment in magnetic materials with broad lines and in a cryogenics environment is one month as compared to one day in μSR. Regarding dynamics, the complementarity with μSR is obvious since in NMR there is virtually no end to the experimental time window, except for the stability of the experiment. As such very fast spin dynamics leading to long T_1 can be investigated.

Acknowledgements

It is a pleasure to thank the organizers of the neutron school of the "20^{mes} Journées de la neutronique" who proposed me to make this introduction to the NMR and μSR techniques. It is also a pleasure to acknowledge my colleagues J. Bobroff, E. Kermarrec and P. Mendels for many enlightening discussions and for providing materials for these lecture notes.

References

[1] C.P. Slichter, *Principles of Magnetic Resonance*, Springer Verlag (1978).
[2] E. Fukushima and B.W. Roeder, *Experimental Pulse NMR, A Nuts and Bolts Approach*, Addison-Wesley Publishing Comp. (1981).
[3] S.J. Blundell, *Spin polarized muons in condensed matter physics*, Contemporary Physics 40, 175 (1999) and arXiv:cond-mat/0207699.
[4] A. Yaouanc and P. Dalmas de Réotier, *Muon Spin Rotation, Relaxation, and Resonance, Applications to Condensed Matter*, International series of monographs on physics 147, Oxford Science Publications (2011).
[5] M.H. Cohen and F. Reif, *Solid State Physics*, vol. 5, Seitz and Trunbull ed., Academic Press (1957).
[6] H. Alloul, J. bobroff, M. Gabay and P. Hirschfeld, Rev. Mod. Phys. **81**, 45 (2009).
[7] J. Das, A. Mahajan, J. Bobroff, H. Alloul, F. Alet and E. Sorensen, Phys. Rev. B **69** 144404 (2004).
[8] F. Tedoldi, R. Santachiara and M. Horvatić, Phys. Rev. Lett. **83**, 412 (1999).
[9] J.H. Brewer *et al*, Hyperfine Interactions **63**, 177 (1991).
[10] P. Mendels *et al*, Phys. Rev. Lett. **94**, 136403 (2005).
[11] N. Bloembergen, E.M. Purcell and R.V. Pound, Phys. Rev. **73**, 679 (1948).